# Strong quantum squeezing near the pull-in instability of a nonlinear beam

Ali Passian*
*Computational Sciences and Engineering Division, Oak Ridge National Laboratory, Oak Ridge, Tennessee 37831-6123, USA*

George Siopsis†
*Department of Physics and Astronomy, The University of Tennessee, Knoxville, Tennessee 37996-1200, USA*
(Received 13 October 2015; published 4 August 2016)

Microscopic silicon-based suspended mechanical oscillators, constituting an extremely sensitive force probe, transducer, and actuator, are being increasingly employed in many developing microscopies, spectroscopies, and emerging optomechanical and chem-bio sensors. We predict a significant squeezing in the quantum state of motion of an oscillator constrained as a beam and subject to an electrically induced nonlinearity. By taking into account the quantum noise, the underlying nonlinear dynamics is investigated in both the transient and stationary regimes of the driving force leading to the finding that strongly squeezed states are accessible in the vicinity of the pull-in instability of the oscillator. We discuss a possible application of this strong quantum squeezing as an optomechanical method for detecting broad-spectrum single or low-count photons, and further suggest other novel sensing actions.

DOI: 10.1103/PhysRevA.94.023812

## I. INTRODUCTION

Quantum effects that may be exhibited by mechanical resonators have been of increasing importance, as reported by Blencowe in his review of *quantum electromechanical systems* [1], and more recently by Poot and van der Zant in their review of *mechanical systems in the quantum regime* [2], and by Aspelmeyer *et al.*, in their review of *cavity optomechanics* [3]. In particular, micro- and nanobeams and cantilevers [4–7] have proved highly useful in a host of applications such as photon-oscillator interaction [8] and oscillator-quantum dots coupling [9]. These oscillators have played a central role in the development of several forms of scanning probe microscopy, most notably in the atomic force microscope (AFM) [10–12]. Fabricated typically from silicon or silicon nitrite and coated with thin metallic films of gold or chromium, self-assembled monolayers of biological material such as DNA and aptamers, or other functionalizing materials, microbeams have also been attracting a great deal of interest as biosensors. In a variety of applications such as delayed dynamics [13], optomechanical [14], plasmonic [15], and gas-kinetic forces [16], these oscillators continue to be instrumental to establishing the transition from macro- to microscopic behavior of the studied effects. Employing ultra-thin single crystal silicon cantilevers, sub-atto-Newton force resolution has already been demonstrated in low temperature high vacuum experiments [17]. Apart from the general pursuit of observation of quantum effects in macroscopic systems, understanding and designing oscillators that exhibit superior signal to noise ratio, frequency response and amplitude control can indeed be of great practical importance in sensing and imaging [18], where the ability to sensitively control the response of cantilevers by invoking the properties of their quantum states will lead to a new paradigm in the application domain of such oscillators [2,3]. Ordinarily however, quantum effects are only weakly exhibited by micro- and nanocantilevers. For example, the vibrational energy of a cantilever oscillating in its lowest resonant deformation state (∼kHz) with a typical tip displacement $\sim\mu$m, is only $\sim 10^{-16}$ [J]. Setting the lowest oscillation energy of a cantilever to $\hbar\omega$ yields a tip displacement ∼ a few pm, the measurement of which would typically require a temperature $T \ll \hbar\omega/k_B \sim \mu$K. However, material, geometric, and force-induced nonlinearities can greatly affect the cantilever response and possibly enhance the associated quantum effects. While in principle, an oscillator in one of its flexural modes, say the fundamental eigenmode, can be prepared in its ground state [19], in practice, it is often prepared in an initial state which is close to the ground state, for example by cavity cooling [20–22].

In the case of force-induced nonlinearity, it is well known that microelectromechanical systems (MEMS) subject to an electric potential develop an instability as the voltage increases past a critical value (pull-in instability) [23]. While this is a classical effect, quantum properties of microcantilevers have also been studied for electrically driven cantilevers [24,25], as well as fixed beams near the Euler (buckling) instability [26], and squeezed quantum states were shown to exist (assuming that quantum mechanics applies to such mesoscopic systems). Here we explore the quantum effects near the pull-in instability for the arrangement shown in Fig. 1. Investigation of this highly nonlinear parameter regime is in part motivated by our previous observation of the broadband sensitive scattering properties of passive multilayer thin film dielectric or semiconductor-metal beams [14,15]. Thus, as an application we propose a photon detection scheme based on the strong photoacoustic response to infrared photons by metal coated thin films of silicon nitrite suspended near a substrate, which is here suggested as a candidate system in the presented investigation of the squeezed states. For example, as depicted in Fig. 1, for a ∼5 mm diameter 100 mW output beam of a quantum cascade laser, amplitude modulated at 100 kHz and with a center wavelength of $\lambda = 10\,\mu$m, roughly a fraction of $10^{-10}$ J power will scatter off the surface of a cantilever [14] and engenders a photoacoustic stimulus. Without spectral optimization of the absorption cross

*passianan@ornl.gov
†siopsis@tennessee.edu

 

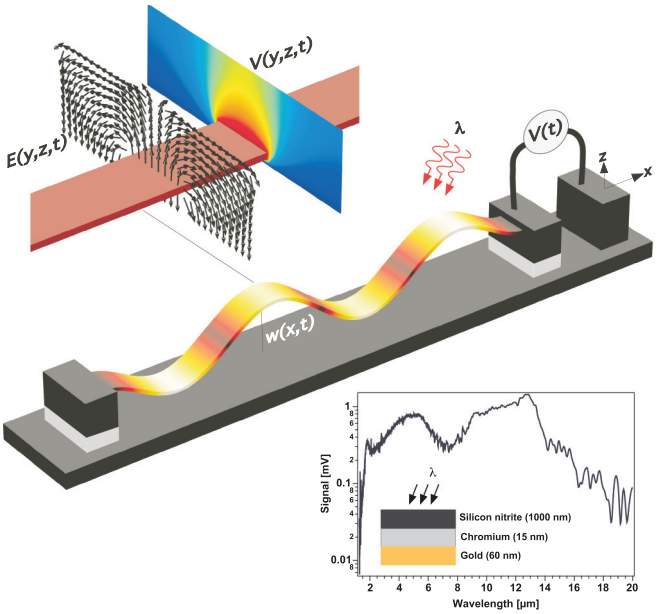


FIG. 1. A polysilicon mechanical oscillator biased to a potential $V(t)$ with respect to a substrate. Response to both mechanical and electric excitation can be computationally obtained by solving the coupled elastodynamic and electrodynamic equations. The computed third displacement eigenmode of the suspended beam is shown as an example along with the potential and field $E$ distributions (top). In a proposed application, low count midinfrared photons are allowed to impinge on the oscillator surface and are subsequently detected via a squeezed quantum deformation state. The spectral response of an example system is shown for silicon nitrite.

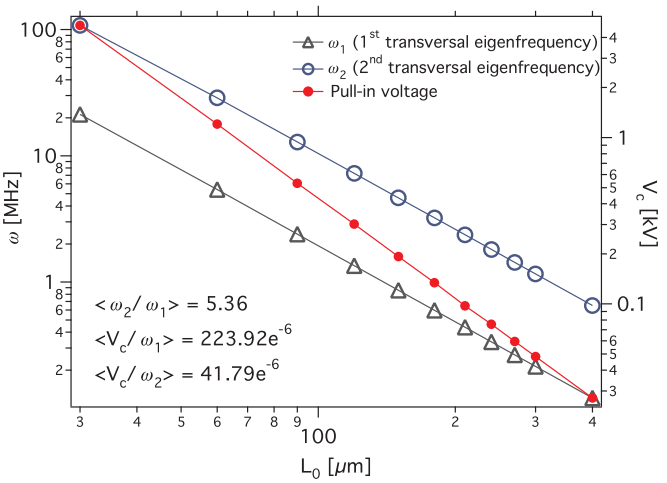


FIG. 2. Critical voltage $V_c$ (right axis) and the undriven undamped resonance frequencies $\omega_1$ and $\omega_2$ (left axis) as functions of $L_0$. The annotations display the averages of the frequency and voltage ratios.

section of the involved materials, a signal $\gtrsim$100 mV can be observed by employing pump-probe reflectometry and lock-in detection under ambient conditions. With optimization, considering a photon energy of $\sim 2 \times 10^{-20}$ J, the detection limit of such a signal would imply a large number of photons ($\sim$million). It is proposed that under the quantum conditions (vacuum, mK cooling, and proper squeezing), this number can be drastically reduced.

In Sec. II we adopt a linear isotropic elastic material (i.e., Hookean stress-strain relations) to formulate the oscillator dynamics but introduce a nonlinearity in the external forces via electrodynamic interactions. By considering the resulting nonlinear dynamics of the beam in Sec. III, we first establish the conditions under which quantum effects may become significant. In doing so we consider a single transversal deformation mode, specifically the fundamental eigenmode of the oscillator and treat the variable describing the position of the beam as an observable so that creation and annihilation operators would alter the quantized oscillation amplitude of the fundamental mode. We then examine the possibility of existence of squeezed states, and therefore investigate whether it is possible to squeeze the oscillation amplitude and phase of a beam oscillating in its fundamental eigenmode without and with being subject to the electrodynamic force nonlinearity. We find that, in the latter case, the squeezing can be made arbitrarily strong as one approaches the pull-in instability. Section VII contains our conclusions and a discussion of the possibility that precision measurements, such as single photon detection capitalizing on mechanical nanometer scale displacement, may benefit from the presented strongly squeezed state.

## II. COMPUTATIONAL AND ANALYTICAL CLASSICAL MODEL

The deformation properties of a planar solid, as formulated in continuum mechanics, can be specialized to describe the dynamics of a polysilicon beam-shaped microstructure with length $0 \leqslant x \leqslant L$, width $-b/2 \leqslant y \leqslant b/2$, and thickness $-d/2 \leqslant z \leqslant d/2$, in an inertial system $xyz$, where it is immobilized at $x = 0$ and $x = L$ and suspended a distance $g_0$ above a planar polysilicon domain, as shown in Fig. 1. Denoting the displacement field with $\mathbf{u}$, the equation of motion in the system shown in Fig. 1 $(i,j = x,y,z)$ for an elastic medium of density $\mu$ subject to a volume force $\mathbf{f}$ is $\mu \partial_{tt} u_i = f_i + \sigma_{ji,j}$, where $\sigma$, proportional to the strain tensor $\epsilon$, is the Cauchy stress tensor, which using the stiffness tensor $\mathbf{c}$ can be expressed via the constitutive equation $\sigma_{ij} = c_{ijkl}\epsilon_{kl}$. The material (polysilicon) considered in this work is assumed to be isotropic and homogeneous, that is, $c_{ijkl} \propto (E,\nu)$, $\forall i,j,k,l$ with $(E,\nu)$ being the Young modulus and Poisson ratio. For a linear material $\epsilon_{ij} = (u_{i,j} + u_{j,i} - u_{k,i}u_{k,j})/2$, which when used with the equation of motion above, one obtains the Cauchy-Navier equation. Fourier transforming the Cauchy-Navier equation expresses it in eigenvalue form $-\mu\omega^2 u_i = f_i + \sigma_{ji,j}$. For practical dimensions $(L,b,d) = (L_0,20,2)$ $\mu$m, with $L_0$ in $\mu$m as a convenient parameter, this equation can be solved numerically [27] for the domain defined in Fig. 1. We computationally obtain an (infinite) eigenfrequency spectrum $\{\omega_n(L_0)\}, n = 1,2,\ldots,$ as shown in Fig. 2 with $f_i = 0$ and damping neglected. For example, $\omega_2(30) = 108.0$ MHz, $\omega_2(90) = 12.9$ MHz, $\omega_1(120) = 7.2$ MHz, etc. can help design a system to achieve a given frequency response. We note that the fluctuation-dissipation theorem establishes a path to obtaining the mode $n$ dependent Brownian oscillation amplitude of the cantilever. In the absence of any explicit driving forces, the cantilever is therefore assumed to possess

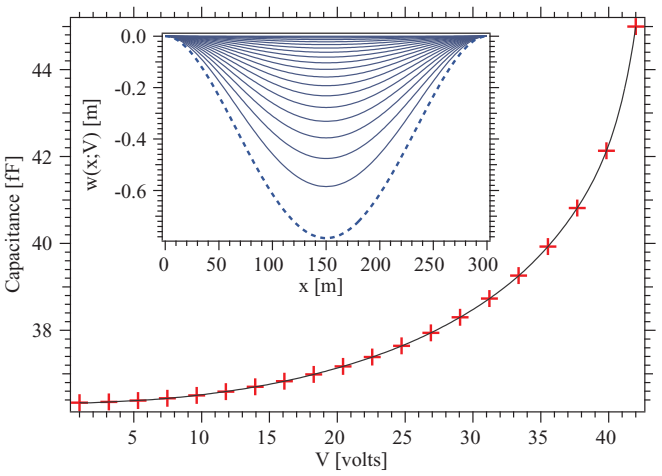


FIG. 3. Capacitance and stationary deformation (inset) of the system as functions of applied potential difference. The dashed curve in the inset shows a midpoint deformation of near −800 nm leading to the pull-in instability at a voltage near 42 V.

sufficient Brownian amplitude to be resonantly excited into low amplitude oscillations with the first few eigenmodes readily observed experimentally [13].

By imposing a time ($t$) dependent harmonic potential difference $V(t)$ between the weakly oscillating (noise driven) cantilever and the substrate, the system can be driven into high amplitude resonance by frequency tuning $\boldsymbol{f}(\omega) = \boldsymbol{V}_0 \sin(\omega t) = \boldsymbol{F}_{\rm drive}$, where $|\boldsymbol{V}_0|$ may be obtained from integrating Maxwell's stress tensor. As shown computationally in Fig. 1 for the third excited eigenmode $\omega \to \omega_3(300)$ and $g_0 = 2$ $\mu$m, the approaching point to the surface (variable gap) will depend on the excited eigenmode. In the stationary case where $V$ is static, solving the coupled Cauchy-Navier and Poisson equations for the transversal displacement component of the neutral axis defined by $(0,0,w)$, we obtain a pull-in instability of just above 42 V, as seen from the capacitance plot in Fig. 3, and from the corresponding displacement as a function of the applied voltage indicating a midpoint deformation of $w|_{x=L_0/2} \approx -800$ nm just before the collapse to the substrate, shown in the inset of Fig. 3. The computed deformation agrees well with the general approximation of the static deformation of a MEMS parallel plate capacitor $\approx g_0/3$ as we are not considering dynamic or resonant pull-in cases [28]. For a fixed $g_0 = 2$ $\mu$m, the onset of instability occurs when $w|_{x=L_0/2} \approx -800$ nm, irrespective of $L_0$. However, the capacitance drops with $L_0$ reduction and the voltage required to induce an instability is computed to scale as shown in Fig. 2. Interestingly, one may observe numerically that $V_c = \alpha_n \omega_n$, where the constants $\alpha_n$ may be extracted from Fig. 2, as annotated.

The computed spectrum of eigenfrequencies $\{\omega_n\}$ for the three-dimensional model includes lateral, longitudinal, transverse, and torsional degrees of freedom. However, the specific arrangement in Fig. 1 permits the negligence of all but the transverse motion, which greatly simplifies (Euler-Bernoulli approximation) the exact equation of motion above to one dimension, allowing an analytical pursuit. Denoting the Lagrangian density with $\mathcal{L}$, we may therefore write the Lagrangian $\mathbf{L} = \int_0^L \mathcal{L} dx$, excluding damping for the moment, with $\mathcal{L} = \mu \dot{w}^2/2 - u(w, w', w'')$, where $\mu$ is now the linear density of the material, and $\dot{w} = \partial w/\partial t$, $w' = \partial w/\partial x$. We consider the possibility that the potential energy of the system $u$ includes the effects of an external force $F_{\rm drive}$. Explicitly, we consider the potential

$$u = \frac{EI}{2}(w'')^2 + \frac{\epsilon_0 V^2}{2} u_e(w), \tag{1}$$

where $I$ is the second moment of inertia, and $\epsilon_0 V^2 u_e$ is the electrostatic potential. The dimensionless quantity $u_e$ is related to the capacitance and is given by [29]

$$u_e = \frac{b}{g_0}\left[\frac{w}{g_0 - w} - \gamma \log\left(1 - \frac{w}{g_0}\right)\right], \quad \gamma = 0.65\frac{g_0}{b}, \tag{2}$$

where $g_0$, defined above, denotes the distance between the substrate and the beam in the undeformed state ($g_0 \ll L$, here $2$ $\mu$m $\ll 300$ $\mu$m). In the absence of deformation ($w \to 0$), the form of the contribution of the capacitor energy to the potential reduces to $(b/g_0^2)\epsilon_0 V^2/2$ with a constant capacitance $\approx$36.3 fF. The equation of motion can be written as

$$\mu \ddot{w} + F_1' - F_2'' = F_{\rm drive}, \tag{3}$$

where $F_1 = -\partial u/\partial w'$, $F_2 = -\partial u/\partial w''$, and $F_{\rm drive} = -\partial u/\partial w$ subject to the boundary conditions:

$$w(0) = w'(0) = w(L) = w'(L) = 0. \tag{4}$$

The explicit form of the equation of motion is obtained by differentiating the potential to get $F_1 = 0$, $F_2 = -EIu''$, and the electrically induced force:

$$F_{\rm drive} = \frac{\epsilon_0 b V^2}{2}\left[\frac{1}{(g_0 - w)^2} + \frac{\gamma}{g_0(g_0 - w)}\right], \tag{5}$$

which puts Eq. (3) into the form (undamped, driven Euler-Bernoulli equation)

$$\mu \ddot{w} + EIw'''' = F_{\rm drive}, \tag{6}$$

which we will treat in both the linear and the nonlinear regimes to prepare for the sought quantization.

In order to solve Eq. (6), we first solve the homogeneous case ($V = 0$), that is, $\mu \ddot{w} + EIw'''' = 0$, by separating the variables with $w = X(x)e^{i\omega t}$, to obtain $X'''' - \lambda^4 X/L^4 = 0$ with $\lambda^4 = \mu\omega^2 L^4/EI$. The solution which satisfies three of the boundary conditions is

$$X(x) = \lambda \sinh\frac{\lambda x}{L} - \lambda \sin\frac{\lambda x}{L} - \lambda\frac{\cosh\lambda - \cos\lambda}{\sinh\lambda + \sin\lambda}\left(\cosh\frac{\lambda x}{L} - \cos\frac{\lambda x}{L}\right). \tag{7}$$

The eigenvalue $\lambda$ is constrained by the fourth boundary condition $X(L) = 0$ to satisfy $\cosh\lambda\cos\lambda = 1$, leading to the discrete spectrum $\lambda = \lambda_1, \lambda_2, \ldots$. Numerically, $\lambda_1 \approx 4.73, \ldots$. Let $\mathcal{X}_n$ be the corresponding normalized eigenfunctions, explicitly

$$\mathcal{X}_n(x) = \frac{\left(\sinh\lambda_n + \sin\lambda_n\right)\left(\sinh\frac{\lambda_n x}{L} - \sin\frac{\lambda_n x}{L}\right)}{\sqrt{\frac{L}{2}(\cosh 2\lambda_n + 2\,\mathrm{sech}\lambda_n - 3)}} - \frac{(\cosh\lambda_n - \cos\lambda_n)\left(\cosh\frac{\lambda_n x}{L} - \cos\frac{\lambda_n x}{L}\right)}{\sqrt{\frac{L}{2}(\cosh 2\lambda_n + 2\,\mathrm{sech}\lambda_n - 3)}}, \tag{8}$$

so that $w(x,t) = \sum_n w_n(x,t) = \sum_n Q_n(t)\mathcal{X}_n(x)$, or explicitly

$$w(x,t) = \sum_{n=1}^{\infty}[A_n\mathcal{X}_n(x)e^{-i\omega_n t} + B_n\mathcal{X}_n(x)e^{i\omega_n t}]. \quad (9)$$

As is observed experimentally in frequency domain from the room temperature and pressure Brownian motion, we assume the system to be in the lowest mode $w_1$ and denote $Q_1(t) = \sqrt{L}q(t)$. The state of the beam is then approximately

$$w(x,t) \approx \sqrt{L}q(t)\mathcal{X}_1(x). \quad (10)$$

Higher modes $n > 1$, which become important at higher temperatures, can be added straightforwardly. For a finite $V$, inclusion of an electrostatic force introduces a nonlinear correction. Integrating the potential yields

$$U = \int_0^L dx\, u \approx \frac{1}{2}m\omega_1^2 q^2 + \frac{\epsilon_0 V^2 L}{2}U_e(q), \quad (11)$$

where $m = \mu L$ is the mass of the cantilever (numerically, $m \approx 30$ ng), and $U_e = \int_0^L dx\, u_e(q\sqrt{L}\mathcal{X}_1)/L$ may be expanded in the small dimensionless quantity $q/g_0$, resulting in

$$U_e = \frac{b}{g_0}\left[0.83(1+\gamma)\frac{q}{g_0} - (2+\gamma)\frac{q^2}{2g_0^2} + 0.44(3+\gamma)\frac{q^3}{g_0^3}\right] + O\left(\frac{q^4}{g_0^4}\right). \quad (12)$$

The minimum of the potential is at $q = \bar{q}$, where $\bar{q}$ satisfies

$$U'(\bar{q}) = m\omega_1^2\bar{q} + \frac{\epsilon_0 V^2 L}{2}U_e'(\bar{q}) = 0. \quad (13)$$

Therefore, small oscillations around the stable equilibrium point $q = \bar{q}$ have frequency $\Omega$, defined as

$$\Omega^2 = \omega_1^2 - \delta^2, \quad \delta^2 = \frac{\epsilon_0 V^2 L(2+\gamma)b}{2mg_0^3}. \quad (14)$$

There is a critical value of the voltage $V = V_c$, for which $U'$ has a double root ($U'' = 0$). In addition to (13), we obtain $\Omega = 0$, which determines the pull-in instability. Numerically, at the pull-in instability, the voltage is $V_c \approx 42$ V, and the displacement is $\bar{q} \approx 1\,\mu$m. For $V > V_c$, there is no equilibrium point ($\Omega^2 < 0$), and (13) has no solution. For $V < V_c$, we have $\Omega^2 > 0$, and (13) has two solutions. The smaller solution corresponds to a stable equilibrium point, whereas the larger one leads to an unstable equilibrium point. We are interested in $V < V_c$ with $V$ close to $V_c$. At the stable equilibrium point, we have oscillations of (small) frequency $\Omega$. In this case, nonlinear effects are significant.

## III. QUANTIZATION AND NOISE

The classical state of the beam [Eq. (9)], under ordinary conditions and without an explicit driving force, can be described by a mixed mode $w = \sum_n w_n$ excited solely by random forces. In this mode, denoting the conjugate momentum density with $\pi = \partial\mathcal{L}/\partial\dot{w} = \mu\dot{w} = \sum_n \pi_n$, or explicitly

$$\pi(x,t) = -i\mu\sum_{n=1}^{\infty}\omega_n[A_n\mathcal{X}_n(x)e^{-i\omega_n t} - B_n\mathcal{X}_n(x)e^{i\omega_n t}], \quad (15)$$

the Hamiltonian is $H = \int_0^L \mathcal{H}dx$, with the density $\mathcal{H} = \pi^2/2\mu + u$. With $w, \pi$ and the coefficients in Eq. (9) promoted to operators, we quantize the system in the absence of an external potential, by imposing equal-time commutation relations

$$[w(x,t),\pi(x',t)] = i\hbar\delta(x-x'),$$
$$[w(x,t),w(x',t)] = [\pi(x,t),\pi(x',t)] = 0. \quad (16)$$

Using Eqs. (9), (15), and (16) we obtain

$$w(x,t) = \sum_{n=1}^{\infty}\sqrt{\frac{\hbar}{2\mu\omega_n}}[b_n\mathcal{X}_n(x)e^{-i\omega_n t} + b_n^\dagger\mathcal{X}_n(x)e^{i\omega_n t}], \quad (17)$$

$$\pi(x,t) = -i\sum_{n=1}^{\infty}\sqrt{\frac{\hbar\mu\omega_n}{2}}[b_n\mathcal{X}_n(x)e^{-i\omega_n t} - b_n^\dagger\mathcal{X}_n(x)e^{i\omega_n t}], \quad (18)$$

where $\omega_n = (\lambda_n/L)^2(EI/\mu)^{1/2}$. At $t = 0$ we deduce

$$b_n = \frac{1}{\sqrt{2\hbar\mu\omega_n}}\int_0^L dx[\mu\omega_n w(x,0) + i\pi(x,0)]\mathcal{X}_n(x), \quad (19)$$

and $b_n^\dagger$ is obtained by conjugation. In terms of the modes $b_n$ and $b_n^\dagger$, the commutation relations (16) read $[b_n, b_m^\dagger] = \delta_{nm}$, and the Hamiltonian, after normal ordering, reads $H = \sum_{n=1}^{\infty}\hbar\omega_n b_n^\dagger b_n$. As alluded to in Eq. (10), at low temperatures, the system behaves approximately as a harmonic oscillator of frequency $\omega_1$, for which we define the operators $q, p$, satisfying $[q,p] = i\hbar$, via

$$q = \sqrt{\frac{\hbar}{2m\omega_1}}(b_1 + b_1^\dagger), \quad p = -i\sqrt{\frac{\hbar m\omega_1}{2}}(b_1 - b_1^\dagger), \quad (20)$$

with quantum fluctuations of the displacement being negligible,

$$\Delta q \sim \sqrt{\frac{\hbar}{m\omega_1}} \sim 0.1 \text{ fm}. \quad (21)$$

Its ground state $|0\rangle_{\omega_1}$ is annihilated by $b_1$. It is easily verified that $q$ defined in (20) is related to the displacement $w$ via Eq. (10) at time $t = 0$. Thus, assuming that the temperature is low enough that other flexural modes are not excited, the quantum state of the system lies in a reduced Hilbert space generated by the creation operator $b_1^\dagger$. Within this subspace, the Hamiltonian simplifies to

$$H_{\text{reduced}} = \frac{p^2}{2m} + \frac{1}{2}m\omega_1^2 q^2 = \hbar\omega_1\left(b_1^\dagger b_1 + \frac{1}{2}\right). \quad (22)$$

If we switch on a constant external potential, then the stable equilibrium point, as implied by Eq. (13), is shifted to $q = \bar{q}$, near which small oscillations occur at frequency $\Omega$, given by Eq. (14). Nonlinearities cause tunneling of the eigenstates of this harmonic oscillator, that is, tunneling of the mechanical degree of freedom in $w$. Although we are interested in approaching the pull-in instability, we will assume that we are sufficiently away from it so that tunneling effects can be neglected over the duration of the experiment. Thus, with an

applied voltage, the Hamiltonian in the Hilbert space of no excitations of higher flexural modes becomes

$$H_{\text{reduced}} = \frac{p^2}{2m} + \frac{1}{2}m\Omega^2(q-\bar{q})^2 = \hbar\Omega\left(a^\dagger a + \frac{1}{2}\right), \quad (23)$$

where we defined the new annihilation operator

$$a = -\alpha + \frac{1}{\sqrt{2\hbar m\Omega}}[m\Omega q + ip], \quad \alpha = \sqrt{\frac{m\Omega}{2\hbar}}\bar{q}, \quad (24)$$

instead of $b_1$ given by Eq. (20). We have $[a,a^\dagger] = 1$ and the ground state of the actuated system $|0\rangle_\Omega$ is annihilated as $a|0\rangle_\Omega = 0$. The Hamiltonian (23) reduces to (22) in the case of vanishing voltage. Quantum fluctuations of the displacement are found, using (21) and (24), to be $\sim 0.1\sqrt{\omega_1/\Omega}$ fm. Thus, they diverge, as we approach the pull-in instability (since $\Omega \to 0$). However, even with $\Omega = 10^{-6}\omega_1$, fluctuations are $\sim$100 fm, therefore still negligible compared to the position of the electrode ($g_0 = 1$ $\mu$m). From Eqs. (20) and (24) we see that the modes in the two cases (with and without applied voltage) are related through the Bogoliubov transformation:

$$b_1 = \cosh r(a+\alpha) + \sinh r(a^\dagger + \alpha), \quad e^{2r} = \frac{\omega_1}{\Omega} > 1. \quad (25)$$

The ground state in the actuated system $|0\rangle_\Omega$ is a *squeezed coherent* state in the system with no applied voltage, and $r$ is the squeezing parameter [30]. If the beam operates near the pull-in instability, $r$ is large. When operated as a sensor, in the presence of an optical or molecular stimulus leading to photothermal or photoacoustic and/or physi- or chemisorption, the beam in the dynamic mode measurement exhibits a frequency shift or a quasistatic displacement in the static mode measurement as a result of a direct or an effective form of mass loading, surface stress variation, asymmetric deformation or swelling (in the case of multilayer beams such as coated microcantilevers), including sensor-environment coupling. The detected frequency shifts or static bending comprise the sensor signal [14,15,31]. Therefore, $r$ can change dramatically, as the system moves away from the pull-in instability.

While characterization of the noise observed in experiments using solid micro- and nanostructures is an on-going effort, typically, temperature and damping effects play a role in the measurement of the response of beam-based sensors. For such sensors, while the exact form of a noise model may not be available without specific experimental verification, reasonable assumptions can be made to account for the effect qualitatively. Thus, in the absence of an applied voltage, if the beam is held at temperature $T$, then it will be in the thermal state

$$\rho = (1-\beta)\sum_{n=0}^{\infty}\beta^n|n\rangle\langle n|, \quad \beta = e^{-\frac{\hbar\omega_1}{k_BT}}, \quad (26)$$

where the states $|n\rangle$ are created with $b_1^\dagger$. The average number of phonons of this mode in the system is

$$\langle n\rangle = \langle b_1^\dagger b_1\rangle = \frac{\text{Tr}[b_1^\dagger b_1\rho]}{\text{Tr}[\rho]} = \frac{\beta}{1-\beta} \approx \frac{k_BT}{\hbar\omega_1}. \quad (27)$$

For $\omega_1/2\pi = 1$ MHz, $T = 10$ mK, we have $\langle n\rangle \approx 220$.

We will now turn on a dc voltage and study the response of the beam. It should be noted that, although we here assume the oscillator to be in its first resonant flexural eigenmode, the same scheme can be applied to any other resonance or off-resonance deformation state of the oscillator with little additional effort.

## IV. PREPARATION OF THE INITIAL STATE

To prepare the proposed system, we form a cavity by invoking a suitable reflective surface of the beam, as depicted in Fig. 4. To achieve high reflectivity, a segment of the top (or bottom) surface of the beam can be appropriately coated (depending on $\omega_0$), for example with a few ($\sim$10) nm of aluminum. The Hamiltonian for such an optomechanical system was derived by Law [32] for the case where the internal modes of the mechanical oscillator can be neglected. In light of Eqs. (22) and (23) however, this Hamiltonian is valid for our study.

We begin by cooling down the system to the mK range. We then purify the thermal state of the system with short laser beam pulses (of duration small compared to the period $\sim 1/\omega_1 \sim 10$ $\mu$s–fs pulses will do) as follows [35,36]. Thus, at the outset, the beam is in the thermal state per Eq. (26). In this state, for the quadratures:

$$X_1 = \frac{1}{\sqrt{2}}(b_1^\dagger + b_1) = \sqrt{\frac{m\omega_1}{\hbar}}q,$$
$$X_2 = \frac{i}{\sqrt{2}}(b_1^\dagger - b_1) = \frac{p}{\sqrt{\hbar m\omega_1}}, \quad (28)$$

we have

$$\langle X_1\rangle = \langle X_2\rangle = 0, \quad \langle X_1^2\rangle = \langle X_2^2\rangle = \frac{1}{2}\frac{1+\beta}{1-\beta} \approx \frac{k_BT}{\hbar\omega_1}, \quad (29)$$

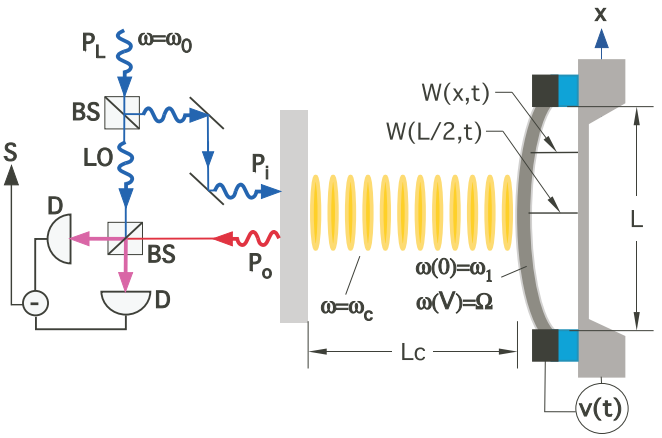


FIG. 4. Cavity optomechanical state preparation and readout of the deformation state of the electrostatically actuated beam employing homodyne detection. Geometric parameters annotated include the distance between the fixed and oscillating mirrors $L_c$, the oscillator length L, and displacement w. The source laser beam $P_L$ of frequency $\omega_0$ and the beam splitter BS provide the local oscillator beam LO, and the cavity input beam $P_i$. With no coupling to the cavity, the oscillator frequency is $\omega_1$ ($\Omega$) prior to (after) switching on V. The cavity output beam $P_o$ and detectors D, generate the difference photocurrent S, which is processed for data acquisition.

with uncertainties

$$\Delta X_1 = \Delta X_2 = \sqrt{\frac{1+\beta}{2(1-\beta)}} \approx \sqrt{\frac{k_B T}{\hbar\omega_1}}. \tag{30}$$

Denoting the $k$th creation and annihilation operators of the cavity field with $a_{L,k}$ and $a^\dagger_{L,k}$, the nonlinear Hamiltonian by Law [32] considers all optical modes $\hbar\sum_k \omega_{c,k} a_{L,k} a^\dagger_{L,k}$. Since in the studied system, shown in Fig. 4, the cavity length is larger than the oscillator displacement, that is, $w(L/2,t) \ll L_c$, our case meets the condition for use of the linearized Hamiltonian [32]. Furthermore, since the oscillator frequencies are smaller than the cavity mode spacing [$\omega(V) \ll \Delta_k \omega_{ck}$], the cavity field is dominated by a single mode [32], which is taken to be closest to resonance with the driving laser [3]. Thus, fixing $k$ and denoting the cavity frequency $\omega_{c,k} = \omega_c$, the interaction Hamiltonian in the frame rotating at the laser frequency $\omega_c \approx \omega_0$ is

$$H_{\rm int} = -\hbar\omega_c a^\dagger_L a_L \frac{q}{L_c}, \tag{31}$$

noting that the radiation force is given by the expectation value of $\hbar\omega_c a^\dagger_L a_L/L_c$. The equation of motion of the optical cavity mode including dissipative effects is given by the Langevin equation

$$\frac{da_L}{dt} = i\omega_c \frac{q}{L_c} a_L - \frac{1}{\tau_c} a_L + \sqrt{\frac{2}{\tau_c}}\theta_L, \tag{32}$$

where $\tau_c$ is the decay time of the cavity ($\tau_c \ll 1/\omega_1$), and the operator $\theta_L$, representing the input noise, obeys commutation relations

$$[\theta_L(t)\ ,\ \theta^\dagger_L(t')] = \delta(t-t'), \tag{33}$$

with correlation functions

$$\langle \theta_L(t)\theta^\dagger_L(t')\rangle = \delta(t-t'). \tag{34}$$

For maximal measurement strength we choose input drive

$$\langle\theta_L\rangle = \sqrt{\frac{N_L}{\tau_c}} e^{-|t|/\tau_c}, \tag{35}$$

where $N_L$ is the mean number of photons in the pulse. Noting that $q$ does not change appreciably during $\tau_c$ since $\omega_1\tau_c \ll 1$, the equation of motion yields

$$\frac{d\langle a_L\rangle}{dt} = -\frac{1}{\tau_c}\langle a_L\rangle + \sqrt{\frac{2}{\tau_c}}\langle\theta_L\rangle, \tag{36}$$

we deduce

$$\langle a_L(t)\rangle = \sqrt{N_L}\left[\frac{1}{\sqrt{2}} + \sqrt{2}\frac{t}{\tau_c}\theta_L(t)\right] e^{-|t|/\tau_c}. \tag{37}$$

From the input-output formulation of cavities [33], relating the far field amplitude outside to the internal cavity field, the output is

$$a_{L,\rm out} = \sqrt{\frac{2}{\tau_c}} a_L - \theta_L. \tag{38}$$

For the phase quadrature

$$P_{L,\rm out} = \frac{i}{\sqrt{2}}(a^\dagger_{L,\rm out} - a_{L,\rm out}) \tag{39}$$

we obtain for large $t$,

$$P_{L,\rm out} \approx \sqrt{2}\omega_c \frac{q}{L}\sqrt{\frac{2}{\tau_c}} e^{-t/\tau_c}\int_{-\infty}^{t} dt' e^{t'/\tau_c}\langle a_L(t')\rangle + \frac{2}{\tau_c} e^{-t/\tau_c}\int_{-\infty}^{t} dt' e^{t'/\tau_c}\theta_L(t') - \theta_L(t). \tag{40}$$

This is measured via homodyne detection, i.e.,

$$P_L = \sqrt{2}\int_{-\infty}^{t} dt' \alpha_{\rm LO}(t') P_{L,\rm out}(t'), \tag{41}$$

where the local oscillator $\alpha_{\rm LO}$ envelope is chosen to match the time dependence of the coefficient of $q$ in the expression for $P_{L,\rm out}$, as

$$\alpha_{\rm LO}(t) = \mathcal{C} e^{-t/\tau_c}\int_{-\infty}^{t} dt' e^{t'/\tau_c}\langle a_L(t')\rangle, \tag{42}$$

where $\mathcal{C}$ is determined by the normalization condition

$$\int_{-\infty}^{+\infty} dt \alpha^2_{\rm LO}(t) = 1.$$

The effect of the measurement, described by the nonunitary operator:

$$Y = \frac{1}{\pi^{1/4}} e^{i\frac{3N_L}{2}\tau_c\omega_c q/L_c - \frac{1}{2}(P_L - \sqrt{10N_L}\tau_c\omega_c q/L_c)^2}, \tag{43}$$

is a change of the state of the beam as

$$\rho \to Y\rho Y^\dagger. \tag{44}$$

We apply two pulses and corresponding homodyne measurements at times $t_1 = \frac{\pi}{2\omega_1}$ and $t_2 = 2t_1$. To find the resulting state, it is convenient to express the thermal state Eq. (26) in terms of coherent states $|\alpha\rangle$ as [34]

$$\rho = \frac{1-\beta}{\pi\beta}\int d^2\alpha e^{-\frac{1-\beta}{\beta}|\alpha|^2}|\alpha\rangle\langle\alpha|, \tag{45}$$

and the operator $Y$ in terms of the quadrature $X_1$ given by Eq. (28)

$$Y = \frac{1}{\pi^{1/4}} e^{i\bar{P}_L X_1 - \frac{1}{2}(P_L - \chi X_1)^2}, \tag{46}$$

where we introduced the dimensionless parameters

$$\bar{P}_L = \frac{3N_L}{2}\omega_c\tau_c\sqrt{\frac{\hbar}{m\omega_1 L_c^2}}, \quad \chi = \omega_c\tau_c\sqrt{\frac{10\hbar N_L}{m\omega_1 L_c^2}}. \tag{47}$$

The average value of an operator $O$ can be written as

$$\langle O\rangle = \frac{1}{Z}\int d^2\alpha e^{-\frac{1-\beta}{\beta}|\alpha|^2}\langle\alpha|Y^\dagger O Y|\alpha\rangle, \tag{48}$$

where

$$Z = \int d^2\alpha e^{-\frac{1-\beta}{\beta}|\alpha|^2}||Y|\alpha\rangle||^2. \tag{49}$$

For explicit calculations we express the states in one of the two quadrature representations. In the $X_1$ representation $X_2 = -i\frac{d}{dX_1}$, and

$$\langle X_1|\alpha\rangle = \frac{1}{\pi^{1/4}} e^{-\frac{1}{2}(X_1-\sqrt{2}\Re\alpha)^2+\sqrt{2}i\Im\alpha X_1}, \tag{50}$$

whereas in the $X_2$ representation $X_1 = i\frac{d}{dX_2}$, and

$$\langle X_2|\alpha\rangle = \frac{1}{\pi^{1/4}} e^{-\frac{1}{2}(X_2-\sqrt{2}\Im\alpha)^2-\sqrt{2}i\Re\alpha X_2}. \tag{51}$$

The first homodyne measurement with outcome $P_{L,1}$ is described by the operator

$$Y_1 = \frac{1}{\pi^{1/4}} e^{i\bar{P}_L X_2 - \frac{1}{2}(P_{L,1}-\chi X_2)^2}. \tag{52}$$

For the quadrature $X_1$ we readily obtain $\langle X_1\rangle = 0$. For the other quadrature we expect $\langle X_2\rangle \propto P_{L,1}$. Taking derivatives and setting $P_{L,1} = 0$, we obtain

$$\langle X_2\rangle = -\left.\frac{d\log Z}{d\chi^2}\right|_{P_{L,1}=0} 2\chi P_{L,1} = \frac{\chi P_{L,1}}{\chi^2 + \frac{1-\beta}{1+\beta}}. \tag{53}$$

For the variances we may set $P_{L,1} = 0$, as they are not affected by the outcome of the measurement. We obtain

$$(\Delta X_2)^2 = -\left.\frac{d\log Z}{d\chi^2}\right|_{P_{L,1}=0} = \frac{1}{2\left(\chi^2 + \frac{1-\beta}{1+\beta}\right)}. \tag{54}$$

The calculation of the other variance $\Delta X_1$ is somewhat involved. Working in the second quadrature representation, after some algebra, we obtain

$$(\Delta X_1)^2 = \frac{1}{2}\left(\chi^2 + \frac{1+\beta}{2(1-\beta)}\right). \tag{55}$$

Without the coupling ($\chi = 0$), we recover our earlier result (30). For $\chi > 1$, the measurement has resulted in squeezing of the $X_2$ quadrature below the ground state noise. The wave function is now much closer to a minimum uncertainty wave packet. For large $\chi$, $\Delta X_2$ approaches zero, whereas $\Delta X_1$ diverges, while

$$\Delta X_1 \Delta X_2 \approx \tfrac{1}{2}, \tag{56}$$

which is independent of the temperature (for sufficiently high $\chi$), to be compared with $\Delta X_1 \Delta X_2 = \frac{1+\beta}{2(1-\beta)}$ before the measurement.

At time $t_2 = \frac{\pi}{\omega_1}$ we perform a second homodyne detection with outcome $P_{L,2}$. The state of the system becomes

$$\rho_0 \propto Y_2 Y_1 \rho Y_1^\dagger Y_2^\dagger\,, \tag{57}$$

where

$$Y_2 = \frac{1}{\pi^{1/4}} e^{i\bar{P}_L X_1 - \frac{1}{2}(P_{L,2}-\chi X_1)^2}. \tag{58}$$

For the variance of the first quadrature we have

$$(\Delta X_1)^2 = \frac{\int d^2\alpha e^{-\frac{1-\beta}{\beta}|\alpha|^2} ||X_1 e^{-\frac{1}{2}\chi^2 X_2^2} e^{-\frac{1}{2}\chi^2 X_1^2}|\alpha\rangle||^2}{\int d^2\alpha e^{-\frac{1-\beta}{\beta}|\alpha|^2} ||e^{-\frac{1}{2}\chi^2 X_2^2} e^{-\frac{1}{2}\chi^2 X_1^2}|\alpha\rangle||^2}. \tag{59}$$

Using

$$\langle X_1|e^{-\frac{1}{2}\chi^2 X_2^2}|\alpha\rangle = \frac{1}{\pi^{1/4}} e^{-\frac{\frac{1}{2}(X_1-\sqrt{2}\Re\alpha)^2+\sqrt{2}i\Im\alpha X_2+\chi^2\Im\alpha^2}{1+\chi^2}}, \tag{60}$$

we obtain

$$(\Delta X_1)^2 = \frac{\chi^2 + \frac{1+\beta}{1-\beta}}{2\left(1 + \frac{1+\beta}{1-\beta}\chi^2 + \chi^4\right)}. \tag{61}$$

Similarly, for the second quadrature, we obtain

$$(\Delta X_2)^2 = \frac{1 + \frac{1-\beta}{1+\beta}\chi^2 + \chi^4}{2\left(\chi^2 + \frac{1-\beta}{1+\beta}\right)}. \tag{62}$$

The average of the second quadrature $\langle X_2\rangle$ remains the same, whereas for the other quadrature, working as before, we obtain

$$\langle X_1\rangle = \frac{\chi^2 + \frac{1+\beta}{1-\beta}}{1 + \frac{1+\beta}{1-\beta}\chi^2 + \chi^4}\chi P_{L,2}. \tag{63}$$

For large $\chi$, the wave function approaches a minimum uncertainty wave packet, as was the case after the first measurement. The advantage of the second measurement is that the system is close to minimum uncertainly even with moderate coupling ($\chi \sim 1$).

For example, for $\omega_1/(2\pi) = 1$ MHz, $T = 10$ mK, and $\chi = 1.5$, before the measurements, we have $\Delta X_1 = \Delta X_2 = 14.8$. After the first measurement we obtain $\Delta X_1 = 14.9$ and $\Delta X_2 = 0.47$, whereas after the second measurement $\Delta X_1 = 0.47$ and $\Delta X_2 = 1.16$. Notice that $\Delta X_1 \Delta X_2 = 0.55$, which is within 10% of the minimum 0.5. A moderate increase in the coupling to $\chi = 3.5$ squeezes the first quadrature to $\Delta X_1 = 0.2$ and $\Delta X_1 \Delta X_2 = 0.502$. Details are shown in Fig. 5.

The above discussion ignores thermal noise between the two measurements. This can be safely done as long as the average number of phonons $\langle n\rangle \approx \frac{k_B T}{\hbar\omega_1}$ is small compared with the mechanical quality factor $\frac{k_B T}{\hbar\omega_1} \lesssim Q$. For $Q \sim 10^4$, this is indeed the case, because $\frac{k_B T}{\hbar\omega_1} \approx 220$.

## V. QUANTUM EVOLUTION

Now switch on a dc voltage $V = V_0$. In the sudden approximation, the initial state of the system will be as discussed above, built on the ground state $|0\rangle_{\omega_1}$. The latter, however, is not annihilated by $a$ [Eq. (24)]. Instead, it is a *squeezed* state.

After we switch on the voltage, for the quadratures

$$X_1' = \frac{1}{\sqrt{2}}(a^\dagger + a) = e^{-r} X_1,$$
$$X_2' = \frac{i}{\sqrt{2}}(a^\dagger - a) = e^{r} X_2, \tag{64}$$

we have

$$(\Delta X_1)^2 = e^{-2r}\frac{\chi^2 + \frac{1+\beta}{1-\beta}}{2\left(1 + \frac{1+\beta}{1-\beta}\chi^2 + \chi^4\right)},$$
$$(\Delta X_2)^2 = e^{2r}\frac{1 + \frac{1-\beta}{1+\beta}\chi^2 + \chi^4}{2\left(\chi^2 + \frac{1-\beta}{1+\beta}\right)}. \tag{65}$$

As the voltage is tuned to its value near (but below) the pull-in instability, we have $\Omega \to 0$, therefore, $\Delta X_1$ can be made very small and $\Delta X_2$ very large with the product $\Delta X_1 \Delta X_2$

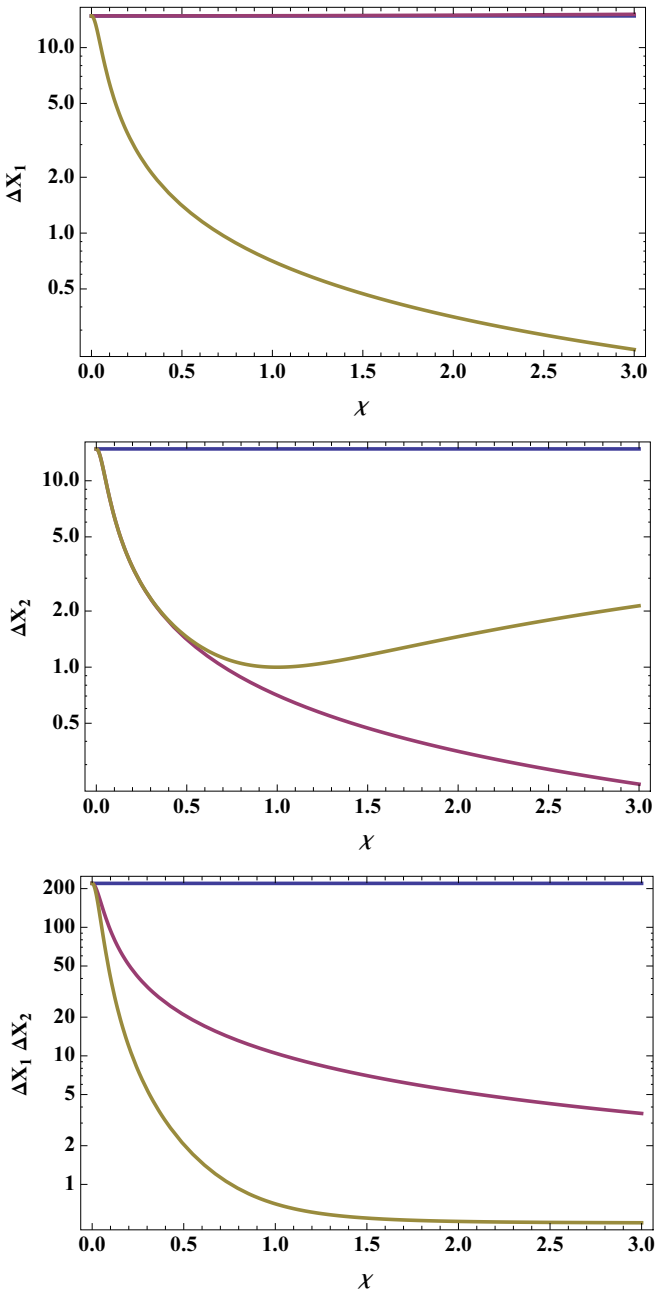


FIG. 5. Initial state uncertainties $\Delta X_1$ (upper), $\Delta X_2$ (middle), and their product $\Delta X_1 \Delta X_2$ (lower), vs coupling $\chi$, before any measurements, after the first homodyne measurement, and after the second homodyne measurement, for frequency 1 MHz and temperature 10 mK. Close to minimum uncertainty ($\Delta X_1 \Delta X_2 \approx 0.5$) is attained after the second homodyne measurement even at moderate coupling.

remaining near minimum uncertainty. It is worthy to note that for the typical values of quality factor $Q$ here, the oscillator may exhibit transient oscillation when switching time is considerably smaller than the dominant mode's relaxation time. In Fig. 6 we characterize the ring-down effect for a beam for various finite switching times $t_0$. As can be seen for an oscillator with the fundamental frequency $\approx$1 MHz, the oscillatory response is negligible for switching times $t_0 \gtrsim 0.3$ $\mu$s. Therefore, for a more realistic application of the

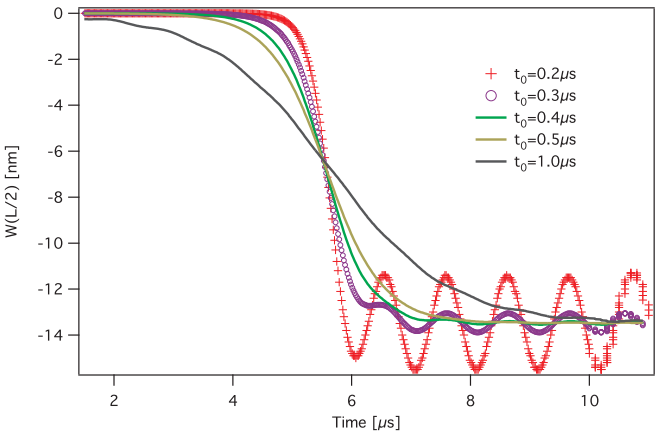


FIG. 6. Characterization of the transient response of the oscillator to the applied bias in a range of switching times. The oscillation period of $\approx$1 $\mu$s for the midpoint displacement $w(L/2)$ observed for switching time $t_0 \geqslant 0.3$ $\mu$s indicates the response (decaying after a few tens of $\mu$s) is primarily dominated by the fundamental mode of the oscillator.

voltage, let $t_0$ be the time over which the voltage is switched on, i.e.,

$$V^2(t) = \frac{V_0^2}{1 + e^{-t/t_0}}, \tag{66}$$

so that $V$ switches from 0, for large negative $t$, say, $t \lesssim -T$, to $V_0$, for large positive $t \gtrsim +T$, with the switch occurring over an interval $t_0$ at $t = 0$. We would like to choose a large enough $T$ so that damping effects can be ignored. As shown in Fig. 2, for a microbeam it is possible to observe $\omega_1 \sim 1$ MHz, and the quality factor can be $Q \sim 10^4$ [13,37], therefore, we may choose $T \lesssim \tau$, where $\tau = Q/\omega_1 \sim 10$ ms is the relaxation time of the system. A fast switch of $t_0 \lesssim \mu$s will then ensure that damping effects can be safely ignored. We note that while design and fabrication of higher $Q$ micro- and nano-oscillators continue to be explored, values of $10^4$ and higher have been reported for a variety of material and geometric considerations [38–42]. From the Heisenberg equations of motion:

$$\frac{dq}{dt} = \frac{1}{i\hbar}[q, \hbar\Omega a^\dagger a], \quad \frac{dp}{dt} = \frac{1}{i\hbar}[p, \hbar\Omega a^\dagger a], \tag{67}$$

we deduce for $q$, measured from its stable equilibrium point $\bar{q}$ (i.e., letting $q \to q - \bar{q}$),

$$\frac{d^2q}{dt^2} + \bar{\Omega}^2(t) q = 0, \quad \bar{\Omega}^2(t) = \omega_1^2 - \frac{\delta^2}{1 + e^{-t/t_0}}, \tag{68}$$

where $\delta$ is the constant voltage shift in frequency defined in (14). The time-dependent frequency $\bar{\Omega}(t)$ smoothly interpolates between $\omega_1$ for $t \to -\infty$ and $\Omega \ll \omega_1$ for $t \to +\infty$. We obtain two linearly independent solutions, $\mathcal{Q}$ and $\mathcal{Q}^*$, where

$$\mathcal{Q}(t) = e^{-i\omega_1 t}\, {}_2F_1(a_+, a_-; 1 + a_+ + a_-; -e^{t/t_0}), \tag{69}$$

with $a_\pm = -i(\omega_1 \pm \Omega)t_0$. Therefore,

$$q(t) = \mathrm{Re} A\mathcal{Q}(t), \quad p(t) = m\dot{q}(t). \tag{70}$$

To determine the coefficient $A$, notice that for large negative time $q(t) \approx \mathrm{Re} A e^{-i\omega_1 t}$ therefore, $A = q(0) + ip(0)/(m\omega_1)$,

i.e., the system is described in terms of creation operators $b_1^\dagger$ [Eq. (20)]. To find $q(t)$ for large positive $t$, we use the hypergeometric identity:

$$
\begin{aligned}
&{}_2F_1(a_+,a_-;1+a_++a_-;-e^{t/t_0})\\
&\quad=\frac{a_-\Gamma(1+a_-+a_+)\Gamma(1+a_--a_+)}{(a_--a_+)2\Gamma^2(1+a_-)}(1+e^{t/t_0})^{-a_+}\\
&\qquad\times{}_2F_1\left(a_+,1+a_-;1+a_+-a_-;\frac{1}{1+e^{t/t_0}}\right)\\
&\qquad+(a_+\leftrightarrow a_-).
\end{aligned}
$$

We obtain $q(t)\approx \mathrm{Re}Be^{i\Omega t}$, where

$$
\begin{aligned}
B=A&\frac{(\Omega-\omega_1)\Gamma(1-2i\omega_1t_0)\Gamma(1+2i\Omega t_0)}{2\Omega\Gamma^2[1-i(\omega_1-\Omega)t_0]}\\
&+(\omega_1\to-\omega_1).
\end{aligned}
$$

For small switch time $t_0\ll 1/\omega_1, 1/\Omega$, we have $B\approx q(0)+ip(0)/(m\Omega)$, i.e., the system is now described by creation operators $a^\dagger$ [Eq. (24)], as expected. The quadratures

$$
X_1=\sqrt{\frac{m}{2\hbar\bar{\Omega}}}\mathrm{Re}[\dot{q}Q-q\dot{Q}],\quad X_2=\sqrt{\frac{m}{2\hbar\bar{\Omega}}}\mathrm{Im}[\dot{q}Q-q\dot{Q}] \tag{71}
$$

smoothly interpolate between the initial and final values of their counterparts in Eqs. (28) and (64), respectively, as the system evolves.

## VI. DETECTION OF THE SQUEEZED STATE

To detect the state of the beam, we apply short pulses and perform homodyne detection. Thus, we obtain the probability distribution of the outcomes

$$
\mathcal{P}(P_L)=\frac{\mathrm{Tr}[Y\rho Y^\dagger]}{\mathrm{Tr}[Y^\dagger Y]}. \tag{72}
$$

If we apply a sequence of pulses at times $\frac{n\pi}{\Omega}$ $(n=0,1,2,\dots)$, then all measurements commute with each other because each one measures the quadrature $X_1$. The duration of each pulse is short, so that evolution of the beam during each pulse can be neglected. We obtain

$$
\mathcal{P}(P_L)=\frac{\mathrm{Tr}[\rho e^{-(P_L-e^r\chi X_1)^2}]}{\mathrm{Tr}[e^{-(P_L-e^r\chi X_1)^2}]}, \tag{73}
$$

from which the state $\rho$ can be reconstructed. Notice that the effective coupling $e^r\chi$ is now strong so the distribution of $P_L$ should closely resemble that of $X_1$.

For comparison, one can perform similar measurements of the beam before the switching on of the voltage (spaced by shorter time intervals $\frac{\pi}{\omega_1}$). In this case, the distribution of the measurement outcomes is

$$
\mathcal{P}(P_L)=\frac{\mathrm{Tr}[\rho_0 e^{-(P_L-\chi X_1)^2}]}{\mathrm{Tr}[e^{-(P_L-\chi X_1)^2}]}, \tag{74}
$$

where $\rho_0$ is the initial state of the beam (57). As can be seen in Fig. 7, in comparison with the results in Fig. 5 (middle panel), one achieves, after measuring the initial state, high levels of squeezing even with moderate to weak coupling by fine tuning the voltage $V$.

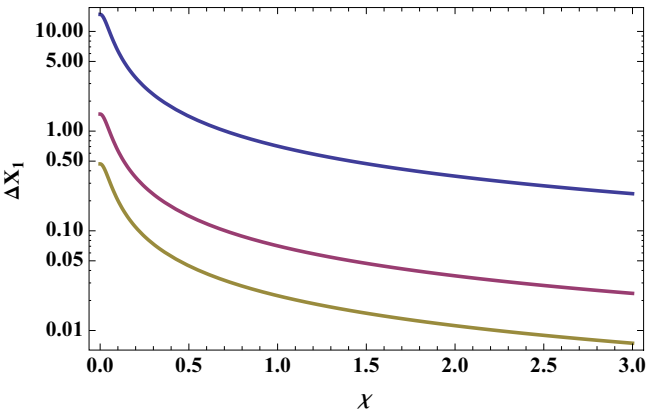


FIG. 7. Uncertainty $\Delta X_1$ before turning on the voltage $V(t)$, and after, for $\Omega=10$ kHz and $\Omega=1$ kHz vs coupling $\chi$. Initial frequency is $\omega_1=1$ MHz, and temperature is 10 mK.

## VII. CONCLUSIONS AND OUTLOOK

In summary, the obtained analytical results, suggesting plausible nonclassical behavior encoded in a single degree of freedom of the studied beam near an electrostatically induced instability point, predict strong squeezing in the transversal displacement $w$. The predicted squeezed states from the presented quantization scheme suggest potential use in devising new sensing capabilities where the pull-in action itself may be utilized as the basis for the signal transduction. In particular, the electrostatically induced nonlinearity that may cause tunneling of the eigenstates near the stable equilibrium point may be proposed as a design route to structures that optimally respond to given field distribution. The possibility of employing such tunneling may lead to new measurement technologies where the actuation mechanism is based on the transition probability among the relevant states. In such instances, one would advantageously employ the squeezed states to better assess the transition of the stable to unstable oscillations. Following the presentation here, one may further consider the possibility of an entangled state where the oscillator is prepared to oscillate at two quantized flexural eignmodes, for example by amplitude modulation of $V(t)$ to achieve the needed Fourier content. The preliminary computational solutions of the classical model for the studied capacitive microbridge proved useful by providing the oscillation eigenfrequency spectrum $\{\omega_n\}$ and the corresponding eigenmodes $\{X_n\}$, the stationary response $w$ and capacitance $C$ as functions of the applied voltage $V$ with the prediction of a threshold value for the pull-in instability. We may conclude that, for design and implementation purposes, a trade-off between the material type, oscillator dimensions, and gap size seems reasonable. For example, fabrication employing graphitic materials with high Young moduli of up to 10 times that of the polysilicon considered here, shorter beams, and narrower gaps will not only affect the spectral positions of the resonances of the system but also greatly impact the threshold voltage. As shown, a material with greater $E$, "blueshifts" the spectrum but also increases the instability threshold voltage. Whereas, for the quantized case, we obtained an analytical expression to account for the contribution of the system's capacitance to the potential energy, in principle, the presented computational

results can be extended to acquire, for a given applied potential $V$, the capacitance as a function of the deformation state $w$. Furthermore, although the classical computational model neglected the stochastic cantilever oscillations, in the quantum calculations, the random noise of the system was taken into account, leading to squeezing when read out by coupling to a cavity. The introduced nonlinearity in the dynamics of the system via imposition of the potential difference $V$, allowed for preparing the oscillator near the pull-in instability where strong squeezing was predicted when read out from cavity-based measurements. The presented approach can readily be adopted to explore the quantum states of other solid and MEMS oscillators. Indeed, with the exception of a modification to Eq. (4), the calculation may be repeated to characterize the squeezed states of cantilevers. One may have then to resort to higher resonances ($n$) of the system since typically for the same materials and dimensions, the spectrum $\{\omega_n\}$ of a cantilever (fixed-free beam) is down-shifted when compared to a bridge (fixed-fixed beam), and consequently, a significantly lower threshold voltage would be required to reach a pull-in instability. Furthermore, the results suggest squeezed displacement in other degrees of freedom may provide a significantly more versatile dynamics since the frequencies of the torsional, longitudinal, and lateral oscillation eigenmodes are not only sufficiently well separated but also typically higher than those of the transversal motion. Advanced fabrication will then have to be employed to create MEMS with nonuniform or asymmetric geometries to allow electrostatic access to the nontransversal modes. Lastly, as a potential application of the studied system we propose a sensitive photon detection scheme. When $V \neq 0$, subjecting the system to incoming photons (Fig. 1) can result in highly sensitive static and dynamic mechanical actuation. For a photon contacting the surface at $x_0$ at time $t_0$, inducing a photoacoustic effect of magnitude $\mathcal{C}$, a total force $f(x,t) = F_{\text{drive}} + \mathcal{C}\delta(x - x_0)\delta(t - t_0)$ is engendered by a number of processes [43] such as carrier generation, plasmon excitation and nonradiative decay, and photothermal absorption depending upon the physical characteristics of the oscillator, for example whether the structure is stratified as a in metal-dielectric thin film or nanoparticle multilayer composite with asymmetric thermal response [14,15]. Without elaborating on the underlying mechanism, it can be shown that the oscillator then undergoes the transient deformation [13] $w(x,t) = \sum_{n=1}^{\infty} \mathcal{I}_n(t)\mathcal{X}_n(x)/\omega_n$, with

$$\mathcal{I}_n(t) = \int_0^1 \mathcal{X}_n(u)\,du \int_0^1 f(u,\tau)e^{-\eta(t-\tau)} \sin\omega_n(t-\tau)\,d\tau,$$

where $\eta$ represents a damping factor.

## ACKNOWLEDGMENTS

We would like to thank M. Blencowe for reading an early version of the manuscript. This research was supported in part by the laboratory directed research and development fund at Oak Ridge National Laboratory (ORNL). ORNL is managed by UT- Battelle, LLC, for the US DOE under Contract DE-AC05- 00OR22725.

[1] M. Blencowe, Phys. Rep. **395**, 159 (2004).
[2] M. Poot and H. S. J. van der Zant, Phys. Rep. **511**, 273 (2012).
[3] M. Aspelmeyer, T. J. Kippenberg, and F. Marquardt, Rev. Mod. Phys. **86**, 1391 (2014).
[4] T. J. Kippenberg and K. J. Vahala, Opt. Express **15**, 17172 (2007).
[5] D. Kleckner, I. Pikovski, E. Jeffrey, L. Ament, E. Eliel, J. van den Brink, and D. Bouwmeester, New J. Phys. **10**, 095020 (2008).
[6] S. Gröblacher, K. Hammerer, M. R. Vanner, and M. Aspelmeyer, Nature (London) **460**, 724 (2009).
[7] E. Finot, A. Passian, and T. Thundat, Sensors **8**, 3497 (2008).
[8] F. Marquardt and S. M. Girvin, Physics **2**, 40 (2009).
[9] Z.-Z. Li, S.-H. Ouyang, C.-H. Lam, and J. Q. You, Phys. Rev. B **85**, 235420 (2012).
[10] G. Binnig, C. F. Quate, and Ch. Gerber, Phys. Rev. Lett. **56**, 930 (1986).
[11] L. Tetard, A. Passian, and T. Thundat, Nat. Nanotechnol. **5**, 105 (2010).
[12] L. Tetard, A. Passian, S. Eslami, N. Jalili, R. H. Farahi, and T. Thundat, Phys. Rev. Lett. **106**, 180801 (2011).
[13] A. Passian, A. L. Lereu, D. Yi, S. Barhen, and T. Thundat, Phys. Rev. B **75**, 233403 (2007).
[14] L. Tetard, A. Passian, R. H. Farahi, B. H. Davison, and T. Thundat, Opt. Lett. **36**, 3251 (2011).
[15] L. Tetard, A. Passian, R. H. Farahi, B. H. Davison, A. L. Lereu, and T. Thundat, J. Phys. D **44**, 445102 (2011).
[16] A. Passian, R. J. Warmack, T. L. Ferrell, and T. Thundat, Phys. Rev. Lett. **90**, 124503 (2003).
[17] H. J. Mamin and D. Rugar, Appl. Phys. Lett. **79**, 3358 (2001).
[18] D. Ebeling, H. Hölscher, and B. Anczykowski, Appl. Phys. Lett. **89**, 203511 (2006).
[19] J. Chan, T. P. Mayer Alegre, A. H. Safavi-Naeini, J. T. Hill, A. Krause, S. Gröblacher, M. Aspelmeyer, and O. Painter, Nature (London) **478**, 89 (2011).
[20] C. Höhberger Metzger and K. Karrai, Nature (London) **432**, 1002 (2004).
[21] D. Kleckner and D. Bouwmeester, Nature (London) **444**, 75 (2006).
[22] I. Favero and K. Karrai, Nat. Photon. **3**, 201 (2009).
[23] J. S. Peng, L. Yang, and J. Yang, Smart Mater. Struct. **23**, 065023 (2014).
[24] L. P. Grishchuk and M. V. Sazhin, Zh. Eksp. Teor. Fiz. **84**, 1937 (1983).
[25] M. P. Blencowe and M. N. Wybourne, Physica B **280**, 555 (2000).
[26] A. Kolkiran and G. S. Agarwal, arXiv:cond-mat/0608621.
[27] The computational results are obtained from the finite elements method. The model was developed using Comsol, http://www.comsol.com/.
[28] A. Fargas-Marques, J. Casals-Terré, and A. M. Shkel, JMEMS **16**, 1044 (2007).
[29] S. Krylov, Int. J. Non-Linear Mech. **42**, 626 (2007).

[30] R. Muñoz-Tapia, Am. J. Phys. **61**, 1005 (1993).
[31] E. Finot, A. Fabre, A. Passian, and T. Thundat, Phys. Rev. Appl. **1**, 024001 (2014).
[32] C. K. Law, Phys. Rev. A **51**, 2537 (1995).
[33] D. F. Walls and G. J. Milburn, *Quantum Optics* (Springer, Berlin 2008).
[34] See Glauber-Sudarshan P-distrubution, for example in [33].
[35] M. R. Vanner, I. Pikovski, G. D. Cole, M. S. Kim, Č. Brukner, K. Hammerer, G. J. Milburn, and M. Aspelmeyer, PNAS **108**, 16182 (2011).
[36] M. R. Vanner, I. Pikovski, and M. S. Kim, Ann. Phys. **527**, 15 (2015).
[37] A. N. Cleland and M. L. Roukes, Appl. Phys. Lett. **69**, 2653 (1996).
[38] J. Lübbe, L. Tröger, S. Torbrügge, R. Bechstein, C. Richter, A. Kühnle, and M. Reichling, Meas. Sci. Technol. **21**, 125501 (2010).
[39] K. Y. Yasumura, T. D. Stowe, E. M. Chow, T. Pfafman, T. W. Kenny, B. C. Stipe, and D. Rugar, J. Microelectromech. Syst. **9**, 117 (2000).
[40] A. Gaidarzhy, M. Imboden, and P. Mohantya, J. Rankin, and B. W. Sheldon, Appl. Phys. Lett. **91**, 203503 (2007).
[41] J. Bartolome, A. Cremades, and J. Piqueras, Appl. Phys. Lett. **107**, 191910 (2015).
[42] J. Yang, T. Ono, and M. Esashi, Appl. Phys. Lett. **77**, 3860 (2015).
[43] D. M. Todorović, B. Cretin, Y. Q. Song, and P. Vairac, J. Appl. Phys. **107**, 023516 (2010).